Sección de Física
Universidad de La Laguna

Phase Slips in Spin-Orbit-Coupled Bose-Einstein Condensates.

Radek Vasicek Ruiz

Undergraduate Thesis
Physics Degree
La Laguna, June 2024

Supervised by
Dr. Antonio Muñoz Mateo

Dr. Antonio Muñoz Mateo
Applied Physics
Universidad de La Laguna
38200 La Laguna, Tenerife

Acknowledgments

I am profoundly grateful to my thesis supervisor, Antonio Muñoz Mateo, whose expertise, guidance, and unwavering support have been invaluable throughout this research endeavor. His passion for the subject has inspired and motivated me, enriching my appreciation and understanding of this fascinating realm of physics. His insightful feedback, intellectual rigor, and constant encouragement have played a pivotal role in shaping the direction and depth of this thesis. I am deeply appreciative of his dedication and the time he has invested in mentoring me.

I extend my deepest appreciation to my family for their unwavering support and encouragement throughout my academic journey.

I would like to acknowledge the contributions of my friends and colleagues whose friendship, filled with moments of laughter, stimulating discussions, and shared experiences, have enriched my academic experience immeasurably.

Special thanks to my partner, whose unwavering support and understanding have been a source of strength and encouragement during challenging times. Their consistent belief in my abilities has been a motivating factor in my academic pursuits.

Abstract · Resumen

Abstract

Bose-Einstein condensates (BECs) of ultracold atomic gases have become pivotal for exploring superfluidity and nonlinear dynamics since their initial realization. This study focuses on a two-component pseudo-spin-1/2 BEC with repulsive interparticle interactions in a ring geometry, where persistent currents and phase slips are investigated. We begin with the analysis of stationary states of linearly coupled spin components, obtaining the spectrum of plane waves, which support superfluid particle currents, and their linear excitations, and highlighting the ground state properties. Our main goal concerns the effects of spin-orbit coupling (SOC), which is first analyzed through the single-particle dispersion, and later through nonlinear plane-wave states that show the emergence of different dynamical regimes, or phases, according to the ratio between the linear coupling and the SOC strengths. This allows us to consider the case study of coherent phase slips produced by the exchange of momentum, carried by quantum vortices, between the spin components of the condensate; this is the so-called quantum coherent phase slip, which is the phase equivalent of the macroscopic transfer of particles by the Josephson effect. To this end, numerical simulations of the time-dependent Gross-Pitaevskii equation are performed, both in the absence and in the presence of SOC, that show how the vortex transfer is mediated by soliton-like structures. Our results are put in context with the current research in ultracold gases.

Keywords: *Spinnor Condensate – Josephson Vortices – Phase Slip – Spin-Orbit Coupling.*

Resumen

Los condensados de Bose-Einstein (BECs) de gases atómicos ultrafríos se han vuelto fundamentales para explorar la superfluidez y la dinámica no lineal desde su desde su primera realización experimental. Este trabajo se centra en un BEC de pseudo-espín-1/2 de dos componentes con interacciones repulsivas entre partículas en una geometría de anillo, donde se investigan corrientes persistentes y deslizamientos de fase. Comenzamos con el análisis de estados estacionarios de componentes de espín linealmente acoplados, obteniendo el espectro de ondas planas, que admiten corrientes de partículas superfluidas, y sus excitaciones lineales, destacando las propiedades del estado fundamental. Nuestro objetivo principal concierne a los efectos del acoplamiento espín-órbita (SOC), que primero se analizan a través de la dispersión de partículas individuales, y luego a través de estados no lineales de ondas planas que muestran la aparición de diferentes regímenes dinámicos, o fases, de acuerdo con la relación entre el acoplamiento lineal y las intensidad del SOC. Esto nos permite considerar el estudio del caso de deslizamientos de fase coherentes producidos por el intercambio de momento, llevado a cabo por vórtices cuantizados, entre los componentes de espín del condensado; esto es lo que se conoce como deslizamiento de fase coherente cuántica, que es el equivalente de fase del corrientes macroscópicas de partículas por el efecto Josephson. Con este fin, se realizan simulaciones numéricas de la ecuación de Gross-Pitaevskii dependiente del tiempo, tanto en ausencia como en presencia de SOC, que muestran cómo se media la transferencia de vórtices mediante estructuras similares a solitones.

Palabras clave: *Condensado Spinnor – Josephson Vortices – Deslizamiento de Fase – Acoplamiento Spin-Orbita.*

Phase Slips in Spin-Orbit-Coupled Bose-Einstein Condensates.

Bose-Einstein condensates (BECs) of ultracold atomic gases have become pivotal for exploring superfluidity and nonlinear dynamics since their initial realization. This study focuses on a two-component pseudo-spin-1/2 BEC with repulsive interparticle interactions in a ring geometry, where persistent currents and phase slips are investigated. We begin with the analysis of stationary states of linearly coupled spin components, obtaining the spectrum of plane waves, which support superfluid particle currents, and their linear excitations, and highlighting the ground state properties. Our main goal concerns the effects of spin-orbit coupling (SOC), which is first analyzed through the single-particle dispersion, and later through nonlinear plane-wave states that show the emergence of different dynamical regimes, or phases, according to the ratio between the linear coupling and the SOC strengths. This allows us to consider the case study of coherent phase slips produced by the exchange of momentum, carried by quantum vortices, between the spin components of the condensate; this is the so-called quantum coherent phase slip, which is the phase equivalent of the macroscopic transfer of particles by the Josephson effect. To this end, numerical simulations of the time-dependent Gross-Pitaevskii equation are performed, both in the absence and in the presence of SOC, that show how the vortex transfer is mediated by soliton-like structures. Our results are put in context with the current research in ultracold gases.

CONTENTS

I. INTRODUCTION

Bose-Einstein condensates represent a remarkable quantum phenomenon where a large number of particles occupy the same quantum state. This phenomenon arises after a phase transition that is somewhat analogous to a vapor condensing into a liquid; however, it occurs purely due to quantum mechanics and, for a free gas, it takes place in momentum space rather than in physical space. The onset of BEC appears when the temperature T drops below a critical temperature T_c, which depends on the particle mass m and the particle density $n = N/V$, and it roughly corresponds to the matching of the de Broglie wave length and interparticle distance $\lambda_{\rm dB} \sim n^{-1/3}$ (Pathria, 2016).

The first experimental realizations of BEC in ultracold atomic gases were achieved in 1995 in ^{87}Rb and ^{23}Na dilute atomic gases, by coolind down the atoms in magneto-optical traps up to temperatures of a few nano-Kelvin. Alkali atoms are particularly well-suited for these experiments due to their effective laser cooling and further temperature reduction via evaporative cooling (Pathria, 2016; Pitaevskii and Stringari, 2016). In these dilute gases, where $n \sim 10^{14}$ cm^{-3}, the range of interatomic forces is negligible against the average interparticle distance so that the interparticle interaction can be modeled by two-particle, contact collisions. As a result, the low-energy interaction can be characterized by a single quantity, the s-wave scattering length a, with $a \ll n^{-1/3}$, which enters the interaction strength $g = 4\pi\hbar^2 a/m$ that plays a crucial role in determining the ground state of the condensate (Pitaevskii and Stringari, 2016). For the BEC to be thermodynamically stable, the s-wave scattering length must be positive $a > 0$, ensuring that the system is kept dilute. In the presence of external fields, BECs can also exist in a metastable state even if the scattering length is negative, provided it is sufficiently small.

Since their first observation, BECs have emerged as a powerful experimental platform for investigating waves and excitations in superfluids and nonlinear systems (Pitaevskii and Stringari, 2016). The study of wave-related structures such as solitons and vortices, and their stability, remains an active research area. Advances in experimental techniques have facilitated the creation and examination of diverse states and given access to quantum simulations of other physical systems (Georgescu, 2020).

Persistent currents, a hallmark of superfluidity, have been observed in BECs (Beattie *et al.*, 2013; Ryu *et al.*,

2007). In superconductors they manifest as dissipationless electric currents, while in electrically neutral superfluids produce particle flows without viscosity, as have been realized both in liquid helium and BECs (Pitaevskii and Stringari, 2016). Vortices play a crucial role in the activation of persistent currents in ring geometries, with phase slips occurring due to the transit of vortex structures (Anderson, 1966). A phase slip is characterized by a sudden 2π change in the phase of a superfluid or superconducting order parameter, caused by the movement of quantized vortices through the medium. This phenomenon leads to temporary disruptions of phase coherence and is typically associated with dissipation . Ultracold atoms, as superfluids, can also exhibit phase slips, often by winding the phase through solitonic states, and can generate quantum superpositions of macroscopic flows (Eckel *et al.*, 2014).

Bose-Einstein condensation of ultracold atoms has also enabled the simulation of gauge fields in electrically neutral systems, providing insights into synthetic magnetic responses (Galitski *et al.*, 2019; Lin *et al.*, 2009). In particular, the discovery of synthetic spin–orbit coupling (SOC) in ultracold atoms has opened up new avenues of research in spinor BECs (Lin *et al.*, 2011). This coupling refers to the interaction between the internal spin degree of freedom of the atoms (so their intrinsic angular momentum) and their motion, and has been achieved through kinetic effects in atom-light interactions. The latter interactions are realized by counter-propagating Raman laser beams that transfer momentum and couple spin states through two-photon processes. The resulting system is subject to a one-dimensional SOC that equally incorporates the Rashba and Dresselhaus spin-orbit interactions known from solid-state physics (Lin *et al.*, 2011). The introduction of spin into the dynamics of ultracold atoms enables the study of fascinating effects such as the spin Hall effect, spin currents, or physical properties that depends on the system topology.

In the present work, we consider a two-component, interacting bosonic system with pseudo-spin-1/2 in an idealized one-dimensional (1D) ring geometry, where periodic boundary conditions apply. These systems are experimentally realizable in ultracold gas setups, where quasi-1D geometries can be achieved through tight transverse confinement. Within a mean-field framework, based on the Gross-Pitaevskii equation, we study the spectrum of plane-wave states of the system and analyze their linear stability. Afterwards, the spin-orbit coupling is introduced, specifically the type with equal contributions of Dresselhaus and Rashba couplings, as realized in ultracold gas experiments (Lin *et al.*, 2011). We show how the presence of SOC significantly alters the properties of the ground state with respect to the case of just linearly coupled condensates, leading to diverse dynamical phenomena (Recati and Stringari, 2022). Among them, we focus on the transfer of quantum vortices between the spin components of the condensate, or coherent phase slips, by numerically solving the time-dependent Gross-Pitaevskii equation. A similar study in the absence of SOC has been reported in the literature (Gallemí *et al.*, 2015).

This work is structured as follows: Section II introduces pseudo-spin-1/2 BECs, the mean-field energy functional and the corresponding equation of motion for the condensate wave function (or order parameter). Section III details a plane-wave analysis including the ground state properties, as energy and current density; it also introduces a hydrodynamic analysis of the system based on the particle density and superfluid velocity, with emphasis on the continuity equation. Section IV discusses the linear stability analysis of plane waves, both polarized and non-polarized plane waves. Section V introduces spin-orbit-coupled BECs, beginning with the single-particle dispersion relations, following with nonlinear plane-wave states, and finishing with their linear stability. Section VI focuses on our main goal, the investigation of coherent phase slips in spin-orbit-coupled BECs, examining first the known cases without SOC; particular types of solitons involved in the dynamics are discussed. Finally, Section VII summarizes our work. An appendix includes details on the numerical methods and also on the type of solitons found in our numerical simulations.

II. PSEUDO-SPIN-1/2 BECS

En esta sección se describe el sistema de estudio como un condensado de Bose-Einstein (BEC) con pseudo-espín-1/2, compuesto por dos componentes acoplados linealmente en una configuración geométrica de anillo. Se detalla el modelo teórico utilizado para describir la dinámica del sistema, basado en la densidad Lagrangiana, para obtener la ecuación de movimiento o ecuación de Gross-Pitaevskii.

The system considered is a spinor Bose-Einstein condensate BEC composed of two linearly coupled components arranged in a ring configuration. This system can be obtained from a two-dimensional condensate experiencing a double-well potential with a sharp barrier dividing the two wells. The quantum coherent tunneling through the barrier gives rise to a linear coupling between components (Smerzi *et al.*, 1997).

The Lagrangian density describing the dynamics of this system, assumed to be 1D, is given by:

$$\mathcal{L} = \left(i\hbar\Psi^*\partial_t\Psi - \mathcal{E}\right), \tag{1}$$

where $\Psi(x) = [\Psi_\uparrow(x), \Psi_\downarrow(x)]^T$ represents the complex-valued wave functions associated with the two compo-

nents of the condensate, and $\mathcal{E}$ is the energy density expressed as

$$\mathcal{E} = \sum_{\sigma=\uparrow\downarrow} \left[\frac{\hbar^2}{2m} |\partial_x \Psi_\sigma|^2 + \frac{g}{2} |\Psi_\sigma|^4 + V(x) |\Psi_\sigma|^2 \right] - \nu \left(\Psi_\uparrow^* \Psi_\downarrow + \Psi_\downarrow^* \Psi_\uparrow \right). \quad (2)$$

Here the terms, in sequence, denote the kinetic energy, the interparticle interaction energy of strength $g > 0$, energy of the external-potential $V(x)$ affecting the 1D system, and finally, the linear coupling term, which introduces a coherent coupling of characteristic energy ν between the two components and gives rise to a phase correlation between them.

By using the principle of least action, from Eq. (1),

$$\frac{\delta \mathcal{L}}{\delta \Psi^*} = \frac{\partial \mathcal{L}}{\partial \Psi^*} - \frac{\partial}{\partial_x} \frac{\partial \mathcal{L}}{\partial (\partial_x \Psi^*)} = 0, \quad (3)$$

the Gross-Pitaevskii (GP) equation for the system is obtained:

$$i\hbar \partial_t \Psi_\sigma = -\frac{\hbar^2}{2m} \partial_x^2 \Psi_\sigma + g |\Psi_\sigma|^2 \Psi_\sigma + V \Psi_\sigma - \nu \Psi_{\bar{\sigma}}, \quad (4)$$

where the subscript $\sigma = \{\uparrow, \downarrow\}$ represents one of the components, while $\bar{\sigma}$ signifies the other component. Notice that this is a nonlinear equation in the condensate wave function due to the interaction term. We will focus on homogeneous systems, without external potential, that is $V(x) = 0$. Then, Eq. (4) is written in matrix form as:

$$i\hbar \frac{\partial \Psi}{\partial t} = \begin{pmatrix} \frac{\hat{p}^2}{2m} + g |\Psi_\uparrow|^2 & -\nu \\ -\nu & \frac{\hat{p}^2}{2m} + g |\Psi_\downarrow|^2 \end{pmatrix} \Psi, \quad (5)$$

where $\hat{p} = -i\hbar \partial_x$ is the momentum operator.

III. NONLINEAR PLANE WAVES

A continuación se analiza el estado fundamental del sistema. Se estudia la energía total del sistema y la densidad de corriente. Se presentan las ecuaciones de continuidad y se examinan las características de equilibrio para la densidad en los componentes del condensado.

An examination of the GP Eq. (5) suggests the presence of an underlying symmetry, since the absence of external potential in the equations implies the translational invariance of the system. Therefore, we can construct an ansatz composed of plane waves

$$\Psi = \begin{bmatrix} \Psi_\uparrow \\ \Psi_\downarrow \end{bmatrix} = e^{-i\mu t/\hbar} \begin{bmatrix} \sqrt{n_\uparrow} e^{ik_\uparrow x} \\ \sqrt{n_\downarrow} e^{ik_\downarrow x} e^{i\varphi} \end{bmatrix}, \quad (6)$$

with the corresponding normalization relation

$$\oint dx \, |\Psi|^2 = N_\uparrow + N_\downarrow = N, \quad (7)$$

where μ is the chemical potential of the system, $n_{\uparrow,\downarrow}$ are constant particle densities, $k_{\uparrow,\downarrow}$ are constant wave numbers, φ is a constant relative phase, and N is the total number of particles in the system. Due to the presence of the linear coupling, only N, but not the number of particles in each component N_σ, remains conserved, and it results in an identical chemical potential μ for both components (Son and Stephanov, 2002).

From the substitution of Eq. (6) into Eq. (5) the following system of equations is obtained:

$$\begin{aligned} \mu e^{ik_\uparrow x} &= \left(\frac{\hbar^2 k_\uparrow^2}{2m} + g n_\uparrow \right) e^{ik_\uparrow x} - \sqrt{\frac{n_\downarrow}{n_\uparrow}} \nu e^{ik_\downarrow x} e^{i\varphi} \\ \mu e^{ik_\downarrow x} e^{i\varphi} &= \left(\frac{\hbar^2 k_\downarrow^2}{2m} + g n_\downarrow \right) e^{ik_\downarrow} e^{i\varphi} - \sqrt{\frac{n_\uparrow}{n_\downarrow}} \nu e^{ik_\uparrow x}. \end{aligned} \quad (8)$$

Then, it can be seen that the eigenvalue Eq. (8) holds if $k_\uparrow = k_\downarrow = k$ and $\varphi = 0, \pi$, and the associated eigenvectors are

$$\Psi_- = \begin{pmatrix} \sqrt{n_\uparrow} \\ \sqrt{n_\downarrow} \end{pmatrix} e^{ikx} e^{-i\mu_k t/\hbar} \quad (9a)$$

$$\Psi_+ = \begin{pmatrix} \sqrt{n_\uparrow} \\ -\sqrt{n_\downarrow} \end{pmatrix} e^{ikx} e^{-i\mu_k t/\hbar}. \quad (9b)$$

As we show later, while Ψ_- provides the system's ground state when $k = 0$, the wave function Ψ_+, with relative phase $\varphi = \pi$, is an excited state.

From Eq. (8) we find the following condition for the component densities

$$(n_\uparrow - n_\downarrow) \left(g \pm \frac{\nu}{\sqrt{n_\uparrow n_\downarrow}} \right) = 0, \quad (10)$$

where we will refer to $n_s = n_\uparrow - n_\downarrow$ as the spin density. Equation (10) yields two sets of solutions, the first one corresponds to states with equal number of particles in both componentes, $n_\uparrow = n_\downarrow$ and then $N_\uparrow = N_\downarrow$, or (spin) non-polarized states, and the second set corresponds to the (spin) polarized states $N_\uparrow \neq N_\downarrow$. Their spin densities are, respectively,

$$n_s = 0, \quad (11a)$$

$$n_s = n \sqrt{1 - \left(\frac{2\nu}{gn} \right)^2}. \quad (11b)$$

Figure 1 represents the potential values of n_s for specific ratios of the system parameters ν and gn. It demonstrates the potential for density imbalance until reaching

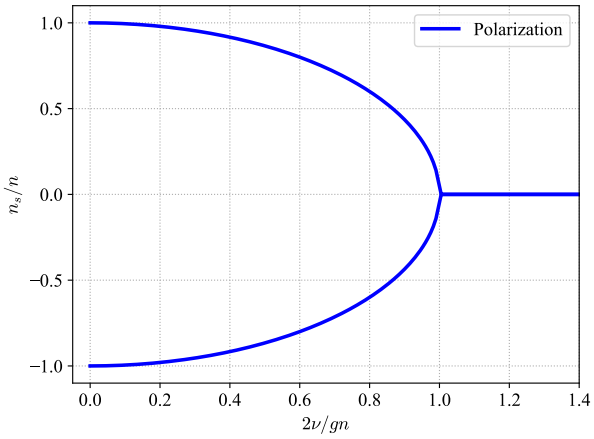

FIG. 1: Spin polarization of plane-wave states, where the spin density $n_s = n_\uparrow - n_\downarrow$ is represented as a function of the ratio $2\nu/gn$ between the linear coupling and the interaction terms. A bifurcation takes place at the critical value $2\nu = gn$ signing the absence of polarized states for $2\nu > gn$.

the critical point $gn = 2\nu$, beyond which the density imbalance becomes forbiden for the system eigenstates.

Moreover, the system's chemical potential is given by the expression: [1]

$$\mu_k = \frac{\hbar^2 k^2}{2m} + \frac{gn}{2} \mp \frac{\nu}{\sqrt{1 - \left(\frac{n_s}{n}\right)^2}}, \tag{12}$$

where $n = n_\uparrow + n_\downarrow$, which in the non-polarized state takes the form

$$\mu_k = \frac{\hbar^2 k^2}{2m} + \frac{gn}{2} \mp \nu. \tag{13}$$

Given that the system is a 1D-ring, with periodic boundary conditions $\psi(x = 0) = \psi(x = 2\pi R)$, the wavevector must satisfy the condition

$$k = \frac{j}{R}, \quad j \in \mathbb{Z}, \tag{14}$$

such that the discrete energy levels have the form

$$\mu_j = \frac{\hbar^2 j^2}{2mR^2} + \frac{gn}{2} \mp \nu, \tag{15}$$

[1] It is important to notice a crucial aspect regarding this expression: in the limit $\frac{n_s}{n} \to 1$ the chemical potential μ_k diverges. This divergence indicates a breakdown in the validity of the model. However, this issue is circumvented by the fact that $n_s/n = 1$ no longer corresponds to an eigenstate of the Hamiltonian.

or, by using the characteristic energy of the ring $\epsilon = \hbar^2/(mR^2)$,

$$\frac{\mu_j}{\epsilon} = \frac{j^2}{2} + \frac{gn/2 \mp \nu}{\epsilon} \tag{16}$$

In figure 2 the dispersion relations of plane waves, μ versus k, are displayed according to Eq. (16).

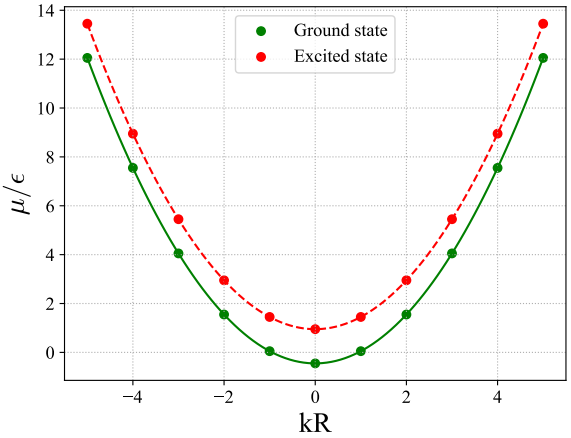

FIG. 2: Dispersion relations of plane waves. Dashed and solid lines (for higher and lower energy states, respectively) serve as visual aids to reveal the functional form of the discrete relationship. Here we are considering $gn/\epsilon = 0.5$ and $\nu/\epsilon = 0.7$

A. Energy

With the energy density of the system, as expressed in Eq. (2), the energy functional is given by

$$E[\Psi] = \sum_{\sigma=\uparrow\downarrow} \int_0^{2\pi R} dx \left[\hbar^2 \frac{|\partial_x \Psi_\sigma|^2}{2m} + \frac{g}{2}|\Psi_\sigma|^4 + V|\Psi_\sigma|^2\right] - \int_0^{2\pi R} \nu \left(\Psi_\uparrow^* \Psi_\downarrow + \Psi_\downarrow^* \Psi_\uparrow\right) dx \tag{17}$$

which, by splitting the wave function as $\Psi = |\Psi| e^{i\theta}$ and considering that there is no external potential $V(x) = 0$, can be rewritten as:

$$E = \sum_{\sigma=\uparrow\downarrow} \oint dx \left\{\frac{\hbar^2}{2m}\left[\partial_x |\Psi_\sigma| + |\Psi_\sigma|(\partial_x \theta)\right]^2 + \frac{g}{2}|\Psi_\sigma|^4\right\} - \oint \nu \left(\Psi_\uparrow^* \Psi_\downarrow + \Psi_\downarrow^* \Psi_\uparrow\right) dx \tag{18}$$

Given that our ground (for $k = 0$) and excited states are described by Eq. (9a) and Eq. (9b), respectively, and considering the inherent boundary condition of the

system described by Eq. (7), we arrive at the energy per particle

$$\frac{E}{N} = \frac{\hbar^2 k^2}{2m} + \frac{gn}{4} - \nu \left[\frac{\nu}{gn} \pm \sqrt{1 - \left(\frac{n_s}{n}\right)^2} \right], \tag{19}$$

which for the unpolarized case $n_s = 0$ takes the value

$$\frac{E}{N} = \frac{\hbar^2 k^2}{2m} + \frac{gn}{4} \mp \nu. \tag{20}$$

B. Current density

The current density of each condensate component can be calculated from the expression

$$J_\sigma = \frac{1}{2m} \left[\Psi_\sigma^* \left(-i\hbar \partial_x \Psi_\sigma \right) + \Psi_\sigma \left(i\hbar \partial_x \Psi_\sigma^* \right) \right] \tag{21}$$

After introducing the systems eigenstates, Eq. (9), the following current densities are found

$$\begin{aligned} J_\uparrow &= \frac{\hbar k}{m} \frac{n + n_s}{2}, \\ J_\downarrow &= \frac{\hbar k}{m} \frac{n - n_s}{2}, \end{aligned} \tag{22}$$

which for the non-polarized case give

$$J_\uparrow = J_\downarrow = \frac{n\hbar k}{2m}. \tag{23}$$

As it is known (Pitaevskii and Stringari, 2016), the superfluid velocity v_x is related to the total current density J by the relation $J = J_\uparrow + J_\downarrow = |\Psi|^2 v_x$, thus from Eq. (22)

$$v_x = \frac{\hbar k}{m}, \tag{24}$$

and it is also given by the definition

$$v_x = \frac{\hbar}{m} \partial_x \theta, \tag{25}$$

where $\partial_x \theta$ refers to the partial spatial derivative of the total phase $\theta = (\theta_\uparrow + \theta_\downarrow)/2$, and $\theta_\sigma = kx - \mu_k t/\hbar$ is the phase of each spin component.

C. Continuity equations

The hydrodynamical analysis of a BEC provides a comprehensive framework that allows for a macroscopic interpretation of the condensate properties. These are given in terms of fluid-like equations of motion that describe the dynamics in terms of the density $|\Psi|^2$ and the velocity v_x fields, or alternatively the current density via $J = |\Psi|^2 v_x$. In particular, by starting with the GP Eqs. (5) expanded as

$$\begin{aligned} i\hbar \partial_t \Psi_\uparrow &= \frac{\hat{p}^2}{2m} \Psi_\uparrow + g|\Psi_\uparrow|^2 \Psi_\uparrow - \nu \Psi_\downarrow, \\ i\hbar \partial_t \Psi_\downarrow &= \frac{\hat{p}^2}{2m} \Psi_\downarrow + g|\Psi_\downarrow|^2 \Psi_\downarrow - \nu \Psi_\uparrow, \end{aligned} \tag{26}$$

and multiplying each equation on the left by the complex-conjugate wave functions, ψ_σ^*, one gets new equations whose imaginary parts give

$$\begin{aligned} \partial_t |\Psi_\uparrow|^2 + \partial_x J_\uparrow &= -\frac{\nu}{\hbar} S_y, \\ \partial_t |\Psi_\downarrow|^2 + \partial_x J_\downarrow &= \frac{\nu}{\hbar} S_y, \end{aligned} \tag{27}$$

where the right sides have been rewritten with the help of Pauli matrices $\{\sigma_x, \sigma_y, \sigma_z\}$ as

$$S_y = i\Psi^* \sigma_y \Psi = \Psi_\uparrow^* \Psi_\downarrow - \Psi_\uparrow \Psi_\downarrow^*. \tag{28}$$

The right hand side of Eq. (27) can also be expressed as $\nu S_y/\hbar = \mathcal{J}$, where

$$\mathcal{J} = \frac{\nu}{\hbar} \sqrt{n_\uparrow n_\downarrow} \sin\varphi = \frac{\nu}{2\hbar} \sqrt{n^2 - n_s^2} \sin\varphi, \tag{29}$$

is the Josephson current modulated by the relative phase $\varphi = \arg \Psi_\uparrow - \arg \Psi_\downarrow$. This is the macroscopic current of particles flipping their spin by means of the Josephson effect (Pitaevskii and Stringari, 2016). The Josephson current is suppressed for in-phase $\varphi = 0$ or phase-opposition $\varphi = \pi$ states.

By adding and subtracting Eqs. (27), we derive the continuity equation for the total density

$$\partial_t n + \partial_x J = 0, \tag{30}$$

where $J = J_\uparrow + J_\downarrow$ is the total current density, and the continuity equation for the spin density n_s

$$\partial_t n_s + \partial_x J_s = 2\mathcal{J}, \tag{31}$$

where $J_s = J_\uparrow - J_\downarrow$ is the spin current density. From Eq. (30), the conservation of the total number of particles $N = N_\uparrow + N_\downarrow$ follows and is constrained by normalization $N = \oint dx n$. Additionally, Eq. (31) highlights the conservation of the population imbalance $N_s = N_\uparrow - N_\downarrow = \oint dx n_s$ only in the absence of net Josephson currents, i.e., for $\oint dx \mathcal{J} = 0$. It is worth noting that in the spinor view, the quantities $n_s = \Psi^\dagger \sigma_z \Psi$ and N_s can be seen as the local M_z and total m_z magnetization, respectively, of a magnetized system; see, e.g. (Recati and Stringari, 2022).

IV. STABILITY ANALYSIS

En esta sección, se analiza la estabilidad de las soluciones estacionarias mediante ecuaciones de Bogoliubov. Se encuentran las frecuencias de excitación para los estados fundamental y excitado, mostrando cómo varían con el momento. Se identifican umbrales de energía y velocidad que definen la estabilidad del sistema frente a perturbaciones externas.

After finding the stationary solutions in the previous section, we proceed with the stability analysis by means of the Bogolibov equations (Pitaevskii and Stringari, 2016). They are obtained from the linearization of the GP Eqs. (5) after adding small perturbartions on the stationary states

$$\Psi(x,t) = \begin{pmatrix} \Psi_\uparrow(x) + \delta_\uparrow(x,t) \\ \Psi_\downarrow(x) + \delta_\downarrow(x,t) \end{pmatrix} e^{-i\mu t/\hbar}, \tag{32}$$

where $\Psi_{\uparrow,\downarrow}(x)$ satisfy the time-independent Eq.(5) with chemical potential μ, and $\delta_{\uparrow,\downarrow}(x,t)$ are generic apace and time dependent small perturbations. Inserting Eq.(32) in Eq.(5) and keeping only the linear terms in $\delta_{\uparrow,\downarrow}$, the following system of equations is obtained:

$$\begin{aligned} i\hbar\partial_t\delta_\uparrow &= -\frac{\hbar^2}{2m}\partial_x^2\delta_\uparrow - \mu\delta_\uparrow + 2g|\Psi_\uparrow|^2\delta_\uparrow + g\Psi_\uparrow^2\delta_\uparrow^* - \nu\delta_\downarrow, \\ i\hbar\partial_t\delta_\downarrow &= -\frac{\hbar^2}{2m}\partial_x^2\delta_\downarrow - \mu\delta_\downarrow + 2g|\Psi_\downarrow|^2\delta_\downarrow + g\Psi_\downarrow^2\delta_\downarrow^* - \nu\delta_\uparrow. \end{aligned} \tag{33}$$

Next, one considers the following form for the perturbations

$$\begin{aligned} \delta_\uparrow(x,t) &= u_\uparrow(x)e^{-i\omega t} + v_\uparrow^*(x)e^{i\omega^* t}, \\ \delta_\downarrow(x,t) &= u_\downarrow(x)e^{-i\omega t} + v_\downarrow^*(x)e^{i\omega^* t}, \end{aligned} \tag{34}$$

such that the excitation energies $\hbar\omega$ and excitation modes $U(x) = [u_\uparrow(x), v_\uparrow(x), u_\downarrow(x), v_\downarrow(x)]^T$ are calculated by solving the linear system

$$B\,U(x) = \hbar\omega\,U(x), \tag{35}$$

where the Bogoliubov matrix B is given by

$$B = \begin{pmatrix} H_\uparrow & g\Psi_\uparrow^2 & -\nu & 0 \\ -g\Psi_\uparrow^{*2} & -H_\uparrow & 0 & \nu \\ -\nu & 0 & H_\downarrow & g\Psi_\downarrow^2 \\ 0 & \nu & -g\Psi_\downarrow^{*2} & -H_\downarrow \end{pmatrix}, \tag{36}$$

and $H_\sigma = -\frac{\hbar^2}{2m}\partial_x^2 - \mu + 2g|\Psi_\sigma|^2$ with $\sigma = \{\uparrow,\downarrow\}$. Dynamical instabilities are related to solutions to Eq. (35) with complex frequencies ω, where the complex part of ω is the rate of exponential growth $\propto \exp[\mathrm{Im}\{\omega\}]$ of the corresponding unstable mode[2]. The inverse of the imaginary part of the unstable frequency can thus be interpreted as the time taken for the mode to grow beyond the perturbative limit.

A. Linear stability of plane waves

The direct substitution of the stationary plane wave states Eq. (9), with chemical potential Eq. (12), into the Bogoliubov Eqs. (35) gives:

$$B_{k,\mp} = \begin{pmatrix} H_{k,\uparrow} & gn_\uparrow e^{i2kx} & -\nu & 0 \\ -gn_\uparrow e^{-i2kx} & -H_{k,\uparrow} & 0 & \nu \\ -\nu & 0 & H_{k,\downarrow} & gn_\downarrow e^{i2kx} \\ 0 & \nu & -gn_\downarrow e^{-i2kx} & -H_{k,\downarrow} \end{pmatrix}, \tag{37}$$

where $H_{k,\uparrow\downarrow} = -\frac{\hbar^2}{2m}\partial_x^2 - \frac{\hbar^2k^2}{2m} + \frac{g}{2}(n \pm 2n_s) \pm \nu/\sqrt{1-(n_s/n)^2}$. To simplify the Bogoliubov matrix and remove the phase factors, we introduce the transformed modes:

$$\begin{aligned} u_j(x) &= \tilde{u}_j(x)e^{ikx}, \\ v_j(x) &= \tilde{v}_j(x)e^{-ikx}. \end{aligned} \tag{38}$$

Next, we expand the perturbations into Fourier modes $\tilde{U}(x) = \tilde{U}_q e^{iqx}$, where, due to the periodic boundary conditions of the 1D ring, the same quantization rule Eq. (14) follows, thus $q = j/R,\ j \in \mathbb{Z}$. This reduces Eq. (37) into

$$\tilde{B}_{\{k,\mp,q\}} = \begin{pmatrix} \epsilon_{kq,\uparrow} & gn_\uparrow & -\nu & 0 \\ -gn_\uparrow & -\bar{\epsilon}_{kq,\uparrow} & 0 & \nu \\ -\nu & 0 & \epsilon_{kq,\downarrow} & -gn_\downarrow \\ 0 & \nu & -gn_\downarrow & -\bar{\epsilon}_{kq,\downarrow}, \end{pmatrix} \tag{39}$$

where:

$$\begin{aligned} \epsilon_{kq,\uparrow\downarrow} &= \frac{\hbar^2}{2m}(q+k)^2 + \frac{g}{2}(n \pm 2n_s) \pm \frac{\nu}{\sqrt{1-\left(\frac{n_s}{n}\right)^2}} - \frac{\hbar^2k^2}{2m} \\ \bar{\epsilon}_{kq,\uparrow\downarrow} &= \frac{\hbar^2}{2m}(q-k)^2 + \frac{g}{2}(n \pm 2n_s) \pm \frac{\nu}{\sqrt{1-\left(\frac{n_s}{n}\right)^2}} - \frac{\hbar^2k^2}{2m}. \end{aligned} \tag{40}$$

Here, the notation $k, \pm$ as subindex denotes the stationary wave vector k under analysis, and whether this state belongs to the lower $(-)$ or upper $(+)$ energy band of the plane-wave spectrum (see Fig. 2).

We focus on the non-polarized states with $n_s = 0$, and find the following eigenvalues of the Bogoliubov matrix Eq. (39):

[2] The symmetry properties of the Bogoliubov equations, as reflected by Eqs. (34), includes both ω and ω^* as eigenvalues

- For the lower energy branch, including the ground state with $k = 0$, $\Psi_{k,-} = \sqrt{\frac{n}{2}} \begin{pmatrix} 1 \\ 1 \end{pmatrix} e^{ikx}$

$$\hbar\omega^{(in)}_{\{k,-\},q} = \frac{\hbar^2 kq}{m} \pm \sqrt{\frac{\hbar^2 q^2}{2m}\left[\frac{\hbar^2 q^2}{2m} + gn\right]} \tag{41a}$$

$$\hbar\omega^{(out)}_{\{k,-\},q} = \frac{\hbar^2 kq}{m} \pm \sqrt{\left(\frac{\hbar^2 q^2}{2m} + 2\nu\right)\left[\frac{\hbar^2 q^2}{2m} + 2\nu + gn\right]} \tag{41b}$$

- For the excited states $\Psi_{k,+} = \sqrt{\frac{n}{2}} \begin{pmatrix} 1 \\ -1 \end{pmatrix} e^{ikx}$

$$\hbar\omega^{(in)}_{\{k,+\},q} = \frac{\hbar^2 kq}{m} \pm \sqrt{\left(\frac{\hbar^2 q^2}{2m} - 2\nu\right)\left[\left(\frac{\hbar^2 q^2}{2m} - 2\nu\right) + gn\right]} \tag{42a}$$

$$\hbar\omega^{(out)}_{\{k,+\},q} = \frac{\hbar^2 kq}{m} \pm \sqrt{\frac{\hbar^2 q^2}{2m}\left(\frac{\hbar^2 q^2}{2m} + gn\right)} \tag{42b}$$

The superscripts indicate the presence of two distinct excitation modes: in-phase and out-of-phase (phase opposition) modes. The in-phase modes correspond to density modes, where the total density n couples strongly to the overall phase θ, while the out-of-phase mode describes a spin mode, where the spin density n_s couples strongly to the relative phase φ (Calderaro *et al.*, 2017); in other words, these modes are associated either with the excitation of total density modulations or of spin density modulations, respectively.

One can recognize the usual Bogoljubov excitation spectrum of scalar condensates (Lamporesi, 2023) (setting here $k = 0$ for the ground state)

$$\hbar^2\omega^2 = \frac{\hbar^2 q^2}{2m}\left(\frac{\hbar^2 q^2}{2m} + gn\right). \tag{43}$$

This excitation spectrum belongs to the in-phase frequency branch of the ground state, and it also appears in the out-of-phase frequency branch of the excited state (when $k = 0$ is set). For low values of the wave number q the dispersion is linear, with slope given by the corresponding speed of sound

$$\lim_{q\to 0} \hbar\omega = \hbar q\sqrt{\frac{gn}{2m}}. \tag{44}$$

Therefore we identify $\sqrt{gn/2m} \equiv c_s$ as the speed of sound of small perturbations in the total density of the condensate. This quantity is relevant for the superfluid properties of the condensate, since excitations with energy $\hbar\omega$ and velocity smaller than c_s cannot excite the system; this is known as the Landau criterion for superfluidity, and forms the basis for the existence of persistent currents (Pitaevskii and Stringari, 2016).

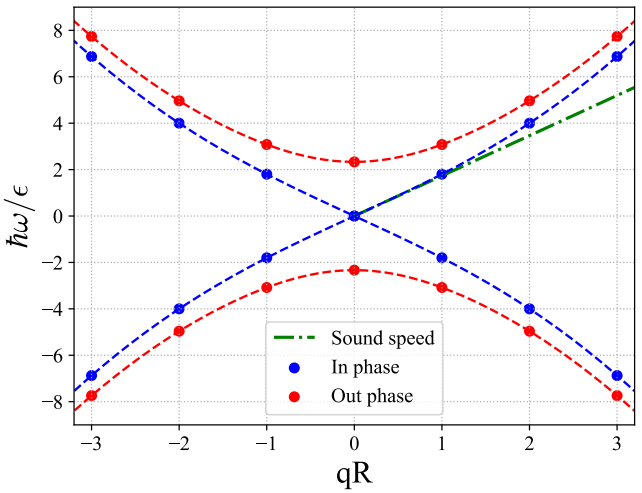

FIG. 3: Energy of Bogoliubov excitations vs. wavenumber $q\,R$ for the system ground state. The dashed lines are visual aids joining the discrete spectrum. The system parameters are $gn = 1.2\varepsilon$ and $\nu = 0.7\varepsilon$.

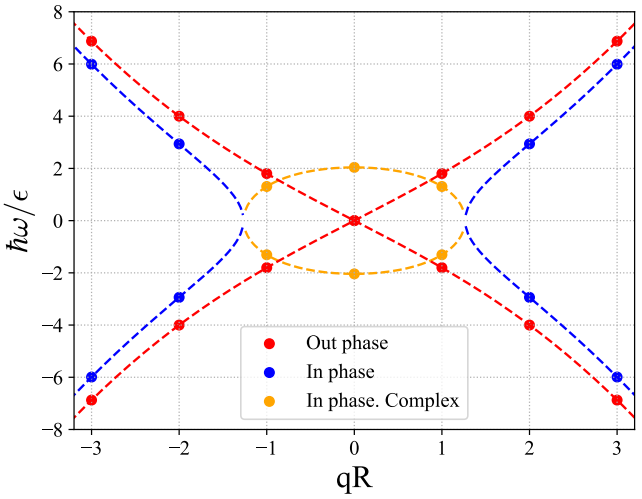

FIG. 4: Energy of Bogoliubov excitations vs. wavenumber $q\,R$ for the branch of excited plane waves at $k = 0$, with a dashed line as a visual aid. The non-zero imaginary part of the frequencies (orange line) correspond to unstable excitation modes. The system parameters are $gn = 1.2\varepsilon$ and $\nu = 0.7\varepsilon$.

Another relevant feature of the system can be found in the upper-energy (or spin) branch of excitation frequencies of the ground state (see Fig. 3), that presents an

energy gap. It depends on the linear coupling ν:

$$\hbar\omega_J = 2\nu\sqrt{1+\frac{gn}{2\nu}}, \tag{45}$$

and corresponds to the Josephson frequency for small amplitude oscillations of the spin density (Abad and Recati, 2013) As c_s, $\hbar\omega_J$ is relevant for the stability of the system, since it defines an energy threshold for the excitation of spin perturbations.

Similarly, one can obtain a gap for the branch of excited plane waves

$$\hbar\omega_{J+} = 2\nu\sqrt{1-\frac{gn}{2\nu}}. \tag{46}$$

but it exists only when $gn < 2\nu$, where the non-polarized states coexist along with polarized states (see Fig. 1). Otherwise, as can be seen in Fig. 4, for $gn > 2\nu$ the in-phase excitation modes produce complex, and thus unstable, excitation frequencies.

V. SPIN-ORBIT-COUPLED BECS

A continuación se introduce el acoplamiento espín-órbita (SOC) en el sistema. Se analiza la dinámica del sistema mediante un Hamiltoniano específico y estudia las soluciones estacionarias. Se estudia la relación de dispersión de energía de partículas únicas y los estados de onda plana no lineales, identificando distintas fases según la intensidad del acoplamiento.

By means of atom-light interactions, spin-orbit-coupled BECs can be realized in electrically neutral ultracold gases (Lin *et al.*, 2011). The dynamics of the resulting systems are ruled by the following Hamiltonian

$$\hat{H} = \frac{1}{2m}\left(\hat{p}I_2 - qA\sigma_z\right)^2 + \frac{gn}{2}I_2 + \left(\frac{gn_s}{2}+\delta\right)\sigma_z + \nu\sigma_x, \tag{47}$$

where $A\sigma_z$ represents the (matrix of the) synthetic gauge field, which couples spin to orbital motion with strength q, and δ is a Zeeman term that shifts the energies of the spinor components.

We will focus on a case with vanishing shift $\delta = 0$, and x-independent gauge fields $qA = \hbar k_\ell$, with characteristic wave number k_ℓ and (recoil) energy $E_\ell = (\hbar k_\ell)^2/(2m)$ (Recati and Stringari, 2022). After dropping constant E_ℓ terms, the Hamiltonian Eq. (47) reads

$$\hat{H} = \begin{pmatrix} \frac{\hat{p}^2}{2m} + g|\Psi_\uparrow|^2 - \frac{\hbar k_\ell}{m}\hat{p} & -\nu \\ -\nu & \frac{\hat{p}^2}{2m} + g|\Psi_\downarrow|^2 + \frac{\hbar k_\ell}{m}\hat{p} \end{pmatrix}. \tag{48}$$

As the Hamiltonian of Section III, this is also translational invariant and then can be solved by plane wave states. It is worth noting that, however, this system is not Galilean invariant, since the transformation to a moving reference frame change the energies of the spin components in a different way.

The energy of the system $E = \oint dx\varepsilon[\Psi] - E_\ell N$ can be written through the energy density functional

$$\varepsilon = \frac{(\hat{\Pi}\Psi)^\dagger\hat{\Pi}\Psi}{2m} + \frac{g(n^2+n_s^2)}{4} - \nu\sqrt{n^2-n_s^2}\cos\varphi, \tag{49}$$

where we have defined $\hat{\Pi} = \hat{p}I_2 - \hbar k_\ell\sigma_z$ as the mechanical momentum operator associated with the velocity of the particles. Furthermore, the continuity equations keep the same form as previously

$$\partial_t n_\uparrow + \partial_x J_\uparrow = -\left(\partial_t n_\downarrow + \partial_x J_\downarrow\right) = \mathcal{J},$$

and the only difference lies in the component current densities J_σ, which include a SOC momentum term,

$$J_\sigma = \mathrm{Re}\left[\Psi_\sigma^*\left(\hat{p} \pm \hbar k_\ell\right)\Psi_\sigma\right]/m. \tag{50}$$

Therefore, the overall and spin continuity equations keep also the same functional form as before.

According to reference (Li *et al.*, 2015), three distinct dynamical regimes, or phases, can be distinguished in the presence of spin-orbit coupling, depending mainly on the parameter

$$\eta = \frac{m\nu}{(\hbar k_\ell)^2}, \tag{51}$$

which is the ratio between the characteristic energies of the linear and SOC couplings. Firstly, for small values of the parameter η, the stripe phase emerges, featured by a ground state that can be understood as a superposition of two plane-wave states with equal weights, which gives rise to the appearance of density modulations in the form of stripes. Secondly, for larger values of the linear coupling, thus of η, the system enters the plane-wave phase, where the ground state settles in a state well described by a single plane-wave state with definite wavenumber $k \neq 0$, the particle density is uniform, and there is spin polarization. Lastly, at even larger values of η, the system reaches the single-minimum phase (also called zero-momentum phase), where the condensate has zero momentum (so can be written as a plane wave with $k = 0$), the density is uniform, and the average spin polarization identically vanishes. We elaborate on the two latter phases by analyzing plane wave states.

A. Single-particle dispersion

Physical insight is gained by examining the noninteracting system. By setting $g = 0$ in the Hamiltonian Eq.

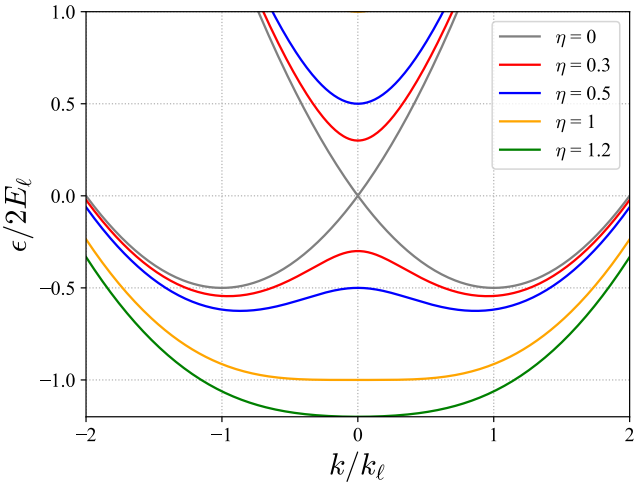

FIG. 5: Single-particle energy dispersion relation as a function of k/k_ℓ across a range of values of the parameter $\eta = m\nu/(\hbar k_\ell)^2$. Two minima at $k \neq 0$ can be observed in the low-energy branch until $\eta < 1$. The upper-energy branch consistently exhibits a single minimum at $k = 0$.

(48), the single particle dispersion relation of plane wave states follows (Lin *et al.*, 2011)

$$\epsilon_k = \frac{\hbar^2 k^2}{2m} \mp \sqrt{\left(\frac{\hbar^2 k_\ell}{m} k\right)^2 + \nu^2}, \tag{52}$$

which is represented in Fig. 5 across a range of values for the non-dimensional ratio $\eta = m\nu/(\hbar k_\ell)^2$. It can be observed that for values of $\nu < (\hbar k_\ell)^2/m$, the low-energy branch ϵ_- exhibits two degenerate minima at wave numbers

$$k_{min} = \pm k_\ell \sqrt{1 - \eta^2}. \tag{53}$$

with non-zero spin density $n_s/n = \pm k_{min}/k_\ell$. In fig 6a, we can observe how by lowering the ratio η the system increases the polarization of the ground state. For $\eta > 1$ the double minima disappear, and the system transitions to a spectrum with a single minimum, that is a non-degenerate ground state at $k = 0$. Regarding the excited energy branch ϵ_+, there is always a single minimum corresponding to $k = 0$.

For generic plane-wave states, Fig. 6b illustrates the spin density change for varying wave number k at fixed values of the ratio η. It shows how a higher momentum leads to a more pronounced difference in component densities. As η increases, indicating a stronger linear coupling ν relative to the spin-orbit coupling k_ℓ, the onset of a total population imbalance is delayed.

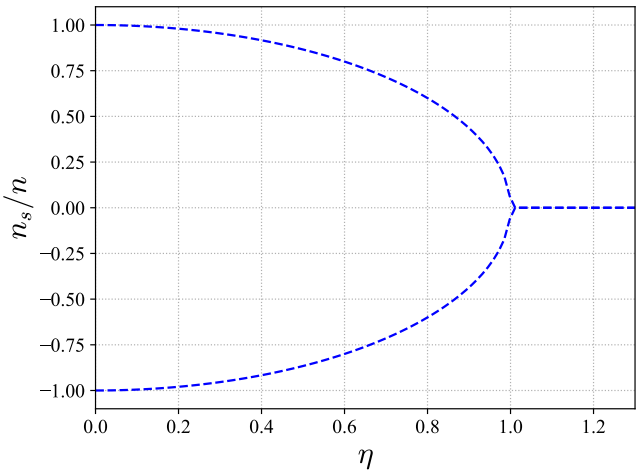

(a) Spin polarization of the ground state in the single particle dispersion as a function of η

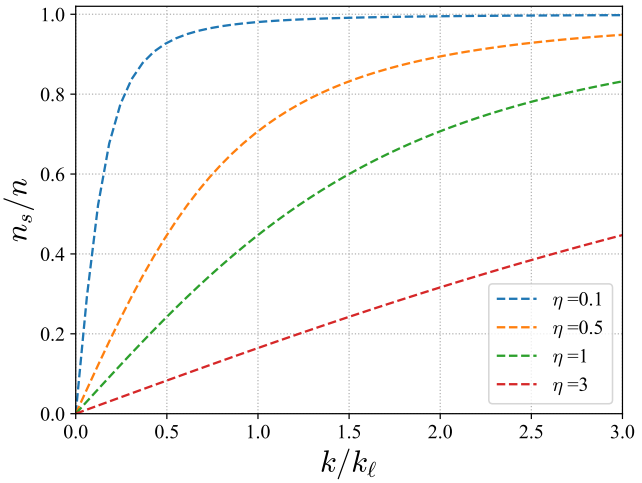

(b) Spin polarization as a function of k/k_ℓ for fixed values of the ratio $0.1 < \eta < 3$.

FIG. 6: Variation of the spin polarization n_s/n in the single particle spectrum of plane waves.

B. Nonlinear plane-wave states

We seek the ground state of the system in the single-minimum or plane-wave phases by employing the same plane-wave ansatz Eq. (6) as in linearly coupled BECs. From its substitution into Eq. (48), one obtains the chemical potential

$$\mu_k = \frac{\hbar^2 k^2}{2m} + \frac{gn}{2} \mp \nu \frac{n}{\sqrt{n^2 - n_s^2}},$$

which takes the same functional form as previously (with $k_\ell = 0$) but it is now constrained by the condition

$$\left(n^2 - n_s^2\right)\left(g n_s - \frac{2\hbar^2 k_\ell}{m} k\right)^2 = 4\nu^2 n_s^2, \tag{54}$$

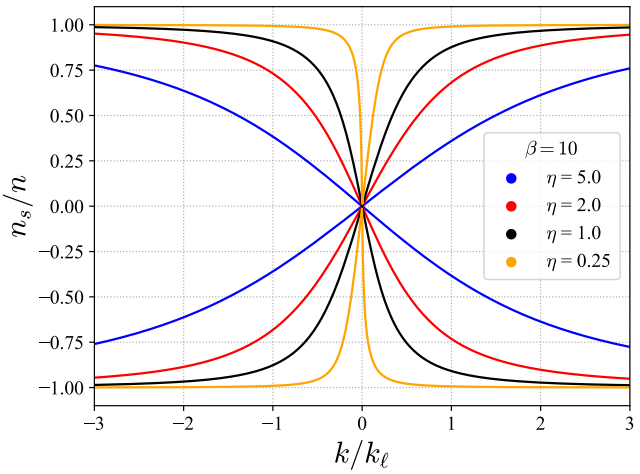

FIG. 7: Numerical solution of Eq. (57) in systems with fixed $\nu/gn = 5$ for a range of values of the parameter η. Increasing values of the spin-orbit coupling enhance the prevalence of fully polarized states.

that manifests the explicit dependence on momentum of the spin density n_s (as in the single-particle case shown before). From Eq. (49) the energy of plane-wave states is

$$\frac{E}{N} = \frac{\hbar^2 k^2}{2m} + \frac{gn}{4}\left[1 + \left(\frac{n_s}{n}\right)^2\right] - \frac{\hbar^2 k_\ell k}{m}\frac{n_s}{n} \mp \nu\sqrt{1 - \left(\frac{n_s}{n}\right)^2}. \tag{55}$$

Upon inspection of Eq. (54), we find that $n_s = 0$ is only possible for $k = 0$, leaving the chemical potential as:

$$\mu_0 = \frac{gn}{2} \mp \nu. \tag{56}$$

For $k \neq 0$, we arrive at a fourth-degree polynomial equation

$$\left(\frac{n_s}{n}\right)^4 - 4\gamma_k\left(\frac{n_s}{n}\right)^3 + \left(\beta^2 + 4\gamma_k^2 - 1\right)\left(\frac{n_s}{n}\right)^2 + 4\gamma_k\left(\frac{n_s}{n}\right) - 4\gamma_k^2 = 0, \tag{57}$$

where we have introduced the parameters

$$\beta = \frac{2\nu}{gn}, \tag{58}$$

$$\gamma_k = \frac{\hbar^2 k_\ell}{mgn}k. \tag{59}$$

When one examines the behavior of Eq. (57) for $n_s/n \to 0$ all the higher order terms vanish, and the polarization becomes linear in momentum $n_s/n \sim \hbar k_\ell/(mgn)\hbar k$. On the other hand, since $\max|n_s/n| = 1$, in the limit of $\gamma_k \gg 1$ (thus $k \gg 1$) the system ends up completely polarized $|n_s/n| \to 1$. From the numerical solution of Eq. (57), one can see that the nonlinear transition of n_s/n (from 0 to 1) takes place in a small range of low momenta. Otherwise, the significant contribution of spin-orbit interaction alters the energy of each component substantially, prohibiting the existence of unpolarized states In what follows, we will focus on systems where $\nu/gn \gg 1$, that is, where the contact interaction strength is not the dominant energy term. Within this regime, figure 7 represents the variation of the spin density with momentum for a range of values of the ratio η. It is evident that an increase in linear coupling reduces the prevalence of fully polarized states.

C. Linear stability for the Single Minimum phase.

The effect of the SOC is also seen in the linear excitations of stationary states, which can be compared with the case of linearly coupled condensates (see Section IV). To this end, we now examine the linear stability of the single minimum phase, whose ground state, characterized by a plane wave with equal density distribution ($n_s = 0$) and zero momentum ($k = 0$), is

$$\Psi_{SM} = \sqrt{\frac{n}{2}}\begin{pmatrix}1\\1\end{pmatrix}e^{-i\mu t/\hbar}, \tag{60}$$

where the chemical potential is given by

$$\mu = \frac{gn}{2} - \nu. \tag{61}$$

The generic Bogoliubov equations, $B\,U(x) = \hbar\omega\,U(x)$, derived from the SOC Hamiltonian given in Eq. (48) lead to the following matrix form:

$$B = \begin{pmatrix} H_\uparrow & g\Psi_\uparrow^2 & -\nu & 0 \\ -g\Psi_\uparrow^{*2} & -H_\uparrow^* & 0 & \nu \\ -\nu & 0 & H_\downarrow & g\Psi_\downarrow^2 \\ 0 & \nu & -g\Psi_\downarrow^{*2} & -H_\downarrow^* \end{pmatrix}, \tag{62}$$

where $H_\sigma = -\frac{\hbar^2}{2m}\partial_x - \mu + 2g|\Psi_\sigma|^2 \pm i\frac{\hbar^2 k_\ell}{m}\partial_x$, with $\sigma = \{\uparrow, \downarrow\}$. From the direct substitution of Eqs. (60-61) into Eq. (62) and the expansion of the linear modes into Fourier modes $U(x) = U_q e^{iqx}$ one obtains

$$B_{SM,q} = \begin{pmatrix} \epsilon_\uparrow & gn/2 & -\nu & 0 \\ -gn/2 & -\epsilon_\downarrow & 0 & \nu \\ -\nu & 0 & \epsilon_\downarrow & gn/2 \\ 0 & \nu & -gn/2 & -\epsilon_\uparrow \end{pmatrix} \tag{63}$$

where $\epsilon_\sigma = \frac{\hbar^2}{2m}(q \mp k_\ell)^2 + \frac{gn}{2} + \nu - E_\ell$. From diagonalization, the dispersion relations are given by:

$$\begin{aligned} \hbar\omega_q^- &= \pm\hbar\sqrt{\omega_q^2 - 2(\Delta\omega_q)^2}, \\ \hbar\omega_q^+ &= \pm\hbar\sqrt{\omega_q^2 + 2(\Delta\omega_q)^2}, \end{aligned} \tag{64}$$

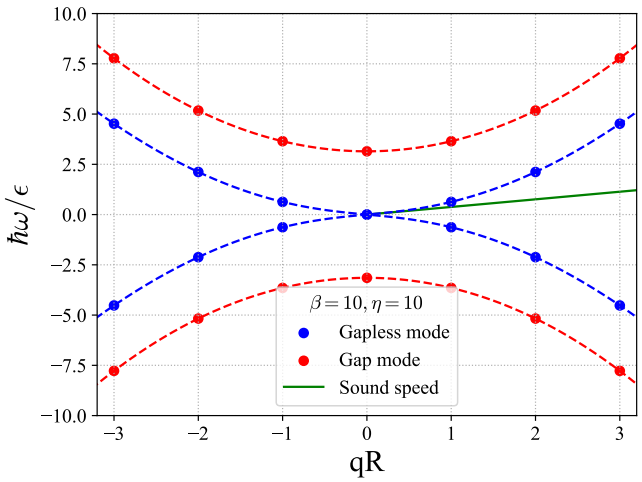

FIG. 8: Dispersion of linear excitations around the ground state in the single minimum phase of a SOC system with $\beta = 10$ and $\eta = 10$.

where

$$(\hbar\omega_q)^2 = \left(\frac{\hbar^2 q^2}{2m} + \nu\right)\left(\frac{\hbar^2 q^2}{2m} + gn + \nu\right) + \left(\frac{\hbar^2 k_\ell q}{m}\right)^2 + \nu^2,$$

$$(\hbar\Delta\omega_q)^4 = \left(\frac{\hbar^2 q^2}{2m} + \frac{gn}{2} + \nu\right)^2 \nu^2 + \left(\frac{\hbar^2 k_\ell q}{m}\right)^2 \left(\frac{\hbar^2 q^2}{2m} + \nu\right)\left(\frac{\hbar^2 q^2}{2m} + gn + \nu\right).$$

While the upper energy branch ω_q^+ presents an energy gap given by

$$\hbar\omega_{gap} = \pm 2\nu\sqrt{1 + \frac{1}{\beta}}, \tag{65}$$

in the same way as in linearly coupled condensates, the lower energy branch ω_q^- tends linearly to zero $\omega_q^- \approx c_s\, q$ for low momentum $q \to 0$, from which the speed of sound is derived as

$$c_s = \sqrt{\frac{gn}{2m}\left(1 - \frac{4E_\ell}{2\nu + gn}\right)}. \tag{66}$$

It is worth comparing this expression with the speed of sound in the absence of SOC; for the same linear coupling and density, the presence of SOC produces a reduction in the speed of sound, therefore a reduction in the range of stability of the superfluid system according to the Landau criterion. When $E_\ell > (2\nu + gn)/4$ superfluidity in the single minimum phase is lost, and the system transits into the stripe phase (Li *et al.*, 2015). Figure 8 shows the excitation branches and the speed of sound for a particular case with $\beta = 5$ and $\eta = 10$.

VI. COHERENT PHASE SLIPS IN SPINOR BECS

Se investigan los deslizamientos de fase coherentes en el sistema, tanto en ausencia como en presencia de acoplamiento espín-órbita. Se utilizan simulaciones numéricas para estudiar la transferencia de vórtices entre los componentes del condensado y se describen diferentes regímenes dinámicos observados.

A phase slip is characterized by a sudden 2π change in the phase of a superfluid or superconducting order parameter. This occurs due to the movement of quantized vortices through the medium; it is typically associated with dissipation, and plays a critical role in the dynamics of superfluidity and superconductivity (Anderson, 1966; Astafiev *et al.*, 2012; Beattie *et al.*, 2013; Eckel *et al.*, 2014).

We investigate the transfer of vortices between the spin components of a pseudo-spin-1/2 BEC by numerically solving the time-dependent Gross-Pitaevskii Eq. (5). Due to the linear coupling, these phase slips in the spin components have not, in general, a dissipative effect, so that the total energy and total momentum of the system are preserved. The Josephson effect is at the basis of the dynamics (Pitaevskii and Stringari, 2016), that here involves the net transfer of phase rather than particles. Persistent currents are initially induced in each component by imprinting linearly varying phases, $\Psi_\sigma \to \Psi_\sigma \times \exp\{iq_\sigma\theta\}$, where $\theta = x/R$ is the azimuthal angle in the ring, and the phases are characterized by different winding numbers $q_\sigma = q_\uparrow, q_\downarrow$ and $q_\uparrow \neq q_\downarrow$. Subsequently, the system state $|q_\uparrow, q_\downarrow\rangle$ is allowed to evolve in time and the spin properties are monitored.

The simulated system comprises two (spin) rings with circumference $L = 11\,\xi$, where $\xi = \hbar/\sqrt{mgn}$ is the characteristic healing length of the system; this setup fixes the ratio between the interaction energy gn and the characteristic energy of the ring, of order $\hbar^2/(mL^2)$, to be $gn = 121\,\hbar^2/(mL^2)$. The initial state is shown in Fig. 9, and it is set to two counter-rotating vortices with winding number $|q| = 1$, i.e $|q_\uparrow = 1, q_\downarrow = -1\rangle$ and equal, uniformly distributed component densities $|\Psi_\uparrow(t=0)|^2 = |\Psi_\downarrow(t=0)|^2 = n/2$.

A. Absence of SOC

We begin with the simpler case without spin-orbit coupling $k_\ell = 0$, focusing on identifying different dynamical regimes based on the characteristic parameter $\beta = 2\nu/(gn)$. As ilustrated in figure 10, three distinct regimes emerge (Gallemí *et al.*, 2015): at high $\beta \gg 1$ an oscillatory regime, with total transfer of momentum between components at frequency $2\nu/\hbar$, can be observed,

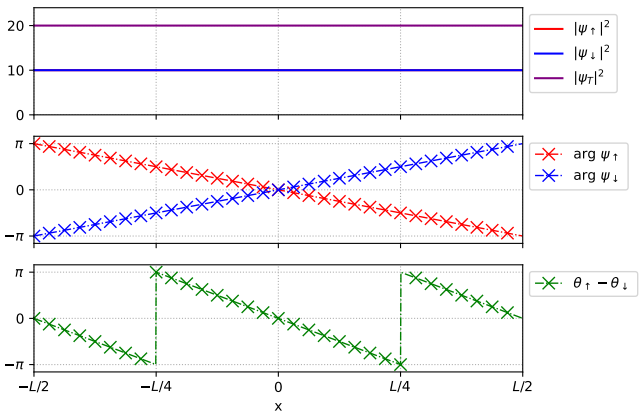

FIG. 9: Density (top), phase (middle), and relative phase (bottom) profiles of the initial state (at $t = 0$) made of two counter rotating vortices with charge (or winding number) $|q| = 1$ that results in a uniform particle density.

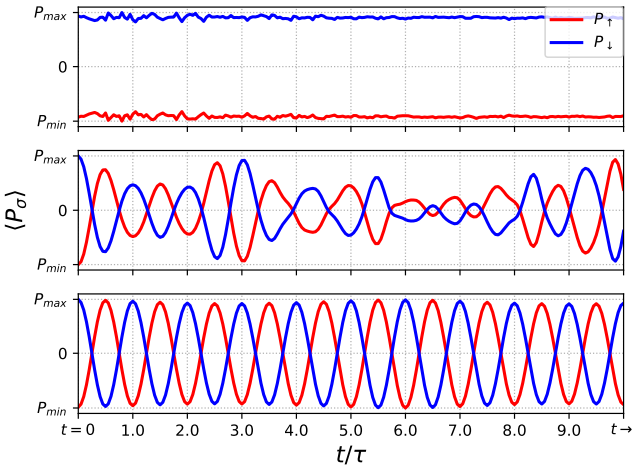

FIG. 10: Dynamical regimes of the momentum transfer between components in a system without SOC. From top to botom: self-trapping with $\beta = 0.01$; transition or NCQPS regime, with $\beta = 1$; and complete momentum transfer or CQPS with $\beta = 10$. For all cases $E_\ell = 0$.

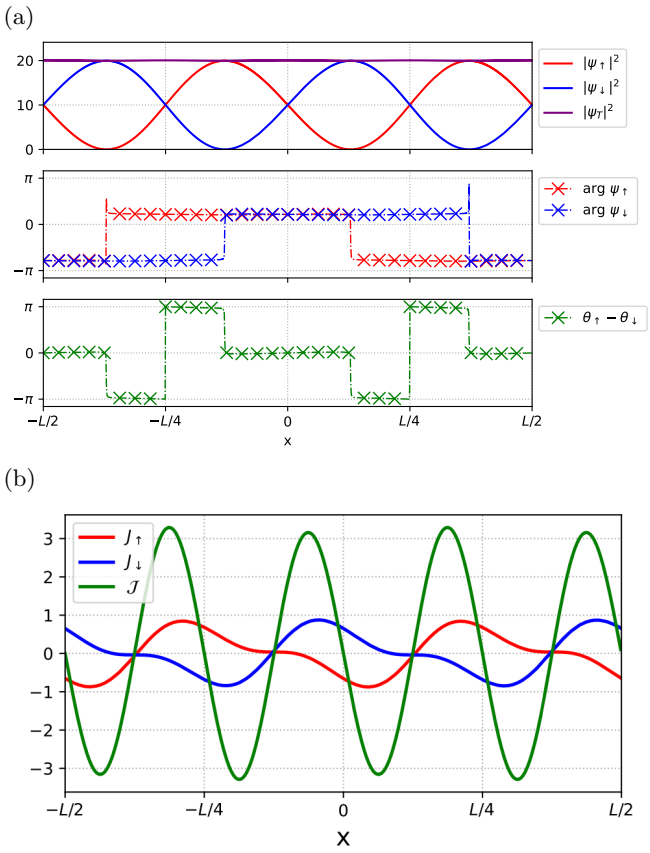

FIG. 11: (a) Same as Fig. 9 for an intermediate time $t = 0.25\,T$ during the time evolution showing the winding number exchange in a system with parameters $\beta = 10, E_\ell = 0$. Two diametrically-opposed density-depleted regions in each component (4 in total) are generated. (b) Current densities (in arbitrary units). The Josephson current $\mathcal{J}$ changes sign at the points of minimum and equal densities.

whereas at low $\beta \ll 1$ no appreciable momentum transfer can be seen; in between, $\beta \sim 1$, an irregular dynamics takes place with partial momentum transfer at non-constant rate. We will refer to these regimes as the coherent quantum phase slip (CQPS) regime, the self trapping regime, and the non-coherent quantum phase slip (NCQPS) regime, respectively.

In order to produce spin excitations, relevant for phase slips in spinor condensates, it is necessary to overcome an energy gap Δ given by (Abad and Recati, 2013; Gallemí *et al.*, 2015) $\Delta = 2\nu\sqrt{1 + 1/\beta}$, which translates into a minimal coupling energy $\hbar\nu_{min}$ required to produce phase slips. In the self-trapping regime, $\beta \ll 1$, this energy gap is not overcome, causing the initial state of the condensate to be essentially preserved during the time evolution. For $\beta \gg 1$ the predominant driving force of coherent phase slips is the linear coupling, which allows the components to completely exchange their winding numbers. The system oscillates at a characteristic frequency $\omega = 2\nu/\hbar$ while the number of particles per component remain unaltered.

During the momentum exchange, local density depletions occur along two perpendicular ring diameters, and each diameter determines two density minima per component [see figure 11(a)]. The density depletions resemble the formation of dark solitons (DSs) with their associated π phase jumps. However, these excitations are better described as Josephson vortices (JVs), which are characterized, apart from the deep depletion in the density profile,

by a 2π-phase jump in the relative phase between components. The main characteristic of the JV is the presence of a localized supercurrent circulation which can be described by persistent currents $J_{\uparrow,\downarrow}(x,t)$ along the components, as well as by tunneling Josephson current $\mathcal{J}$, Eq. (29), between them (Kaurov and Kuklov, 2006). Figure 11(b) presents a snapshot of the condensate currents at the instant of momentum exchange.

B. Presence of SOC

Our analysis primarily investigates a regime where $\beta \gg 1$, ensuring the coherent quantum phase slip (CQPS) evolution of the system. We chose $\beta = 10$ for all subsequent simulations, while varying k_l so that $\eta \in [\infty, 0.15]$. First, by employing imaginary time evolution, we observe that the system's ground state belongs to either the single minimum or the stripe phase, as illustrated in Figure 12. These phases are clearly distinguished by their density modulations or constant density (with zero momentum), respectively.

The spin-orbit coupling significantly influences the dynamics of momentum transfer by inducing a shift of $\pm\hbar k_l$ in the average momentum of each component, as evident from the mechanical momentum equation:

$$\hat{\Pi} = \hat{p} I_2 - \hbar k_\ell \sigma_z,$$

that leads to oscillations around the shifted values. In addition, the variation of the parameter η produces different outcomes, as shown in Figure 13, which depicts the transition from $\eta \gg 1$ (top) to $\eta \sim 1$ (bottom). By decreasing η the amplitude of the oscillations is reduced, and the system transits into a regime with momentum self-trapping; this transition is accompanied by an increasing oscillation frequency, and by a reduction of the Josephson currents.

Although, throughout the condensate's evolution, the number of particles per component remains constant, one can see a pattern of density modulations similar to the case of linearly coupled condensates with two density depletions per component. However, as can be seen in figure 14a, unlike in the case of linearly coupled condensates, the phase profiles show more progressive phase jumps, closer to those of JVs with small Josephson currents. This difference is further illustrated in the current-density profiles of figure 14b.

VII. CONCLUSIONS

In this work, we have investigated the phenomenon of coherent phase slips in spinor Bose-Einstein condensates (BECs), both in the absence and presence of spin-orbit coupling (SOC), through numerical simulations based on the time-dependent Gross-Pitaevskii equation. This

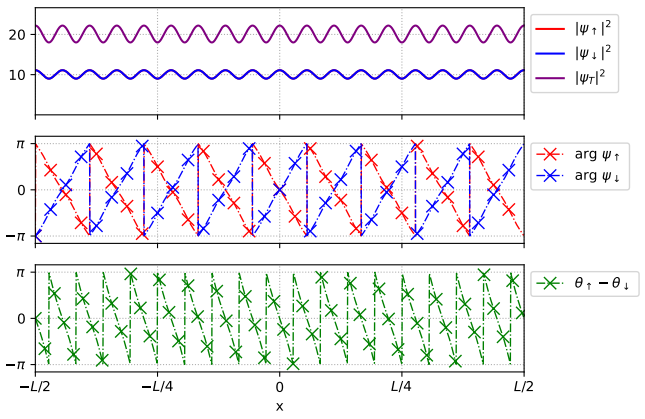

(a) Stripe phase ground state.

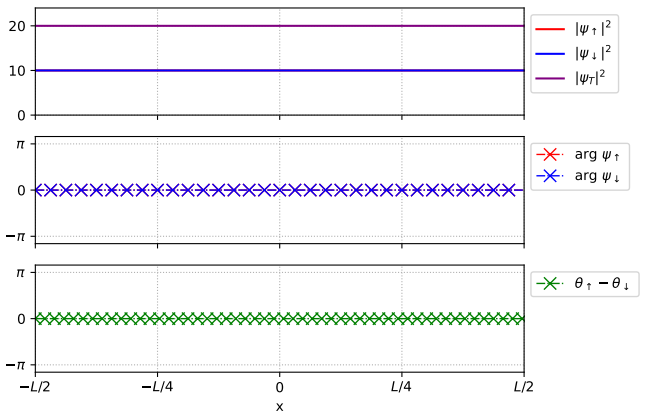

(b) Single Minimum ground state.

FIG. 12: Density and phase profiles of the ground states in the two accessible regimes, stripe (top) and single minimum (bottom) phases, for the exploration of phase-slip dynamics. The system parameters are $\eta = 0.15$ for the stripe phase, and $\eta = 10$ for the single minimum phase, whereas $\beta = 10$ for both cases.

phenomenon has been previously explored in solid-state physics, and also in linearly coupled BECs.

To reach this goal, our work began with the study of spinor condensates made of bosonic atoms that are endowed, by means of atom-laser interactions, with a pseudo-spin-1/2 degree of freedom. The resulting system is well described by two linearly coupled Gross-Pitaevskii equations, where the nonlinearity accounts for the contact interactions between atoms, and the linear coupling allows for spin flips. The various accessible states, the corresponding energies, and the continuity equations of the system were examined, with particular attention paid to plane wave states that support persistent currents.

Since many relevant features of the system can be obtained from the spectrum of excitations of stationary states, we analyzed their linear stability using the Bogoliubov equations that result from small perturbations

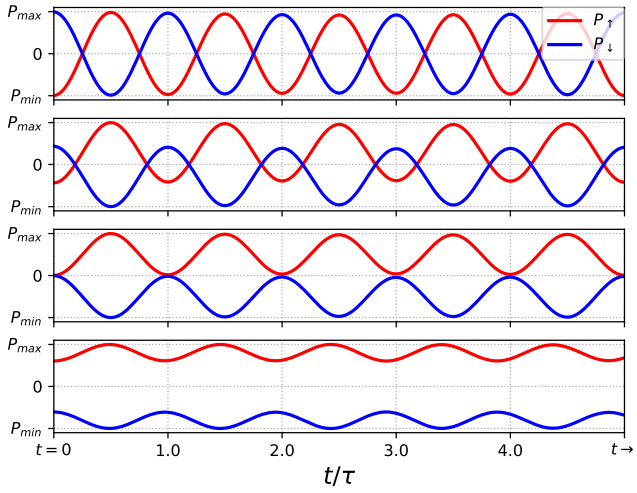

FIG. 13: Oscillations of the mechanical momentum in SOC systems with fixed parameter $\beta = 10$ and varying η. The values range from $\eta = \infty, (k_\ell = 0)$ at the top to $\eta = 1.11$ at the bottom.

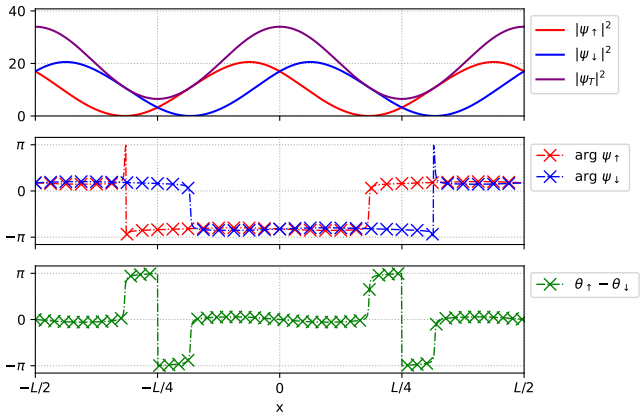

(a) Density and phase profiles showing the formation soliton-like structures with strong density modulations similar to those observed in the absence of SOC.

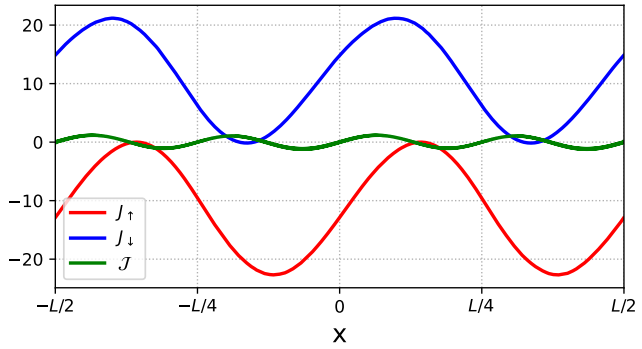

(b) Current-density profiles. The small Josephson currents cannot produce the total exchange of momentum.

FIG. 14: Density, phase, and current-density profiles of an intermediate state during the time evolution of a SOC system with parameters $\beta = 10$ and $\eta = 10$.

on the steady state. By analyzing the dispersion relation of the corresponding excitation modes, we obtained the conditions for dynamical stability based on the real or complex nature of the excitation frequencies. In addition, by paying attention to the low energy (or long wave-length) modes, the speed of sound, and the energy gap between excitation branches were obtained.

After this, we introduced the spin-orbit coupling (SOC) in the system, and showed how the previously mentioned properties (stationary states, linear stability, speed of sound, etc) are modified with respect to the system of linearly coupled condensates. If the latter is well characterized by just one nondimensional parameter $\beta = 2\nu/(gn)$, the presence of SOC introduces a second nondimensional parameter $\eta = m\nu/(\hbar k_\ell)^2$; different values of the pair $\{\beta, \eta\}$ lead the system into distinct dynamical regimes. Our case study on the coherent transfer of vortices between the spin components takes place within two of these regimes, the stripe phase and the single-minimum phase.

In order to gain physical insight, we explored this phase-slip phenomenon in the absence of SOC, revisiting the dynamical scenarios governed by the parameter β, and focusing our attention on cases at high β that are characterized by complete momentum transfer between components. When SOC was introduced, we observed a transition from this situation to a new self-trapping regime (different from the known case that occurs in the absence of SOC) determined by low values of the new parameter η. This transition was marked by the shift from the single minimum to the stripe phase in the ground state of the system. On the other hand, higher values of the SOC lead to higher oscillation frequencies. Throughout the condensate's evolution, SOC did not hinder the formation of solitonic structures (density depletions accompanied by sudden phase jumps) similar to Josephson vortices.

As a whole, our study contributes to understanding the dynamics of coherent phase slips in spinor Bose-Einstein condensates. Further complementary investigations can be suggested, as exploring the impact of different initial states characterized by population imbalance, or investigating systems with attractive (where $g < 0$) interparticle interactions. Finally, the extension of this study from the one-dimensional to two-dimensional space would provide a more realistic approach to experimental conditions.

REFERENCES

Abad, M., and A. Recati (2013), "A study of coherently coupled two-component Bose-Einstein Condensates," arxiv:1301.6864 [cond-mat].

Anderson, P. W. (1966), Rev. Mod. Phys. **38**, 298.

Astafiev, O., L. Ioffe, S. Kafanov, Y. A. Pashkin, K. Y. Arutyunov, D. Shahar, O. Cohen, and J. S. Tsai (2012), Nature **484** (7394), 355.

Baals, C., H. Ott, J. Brand, and A. M. Mateo (2018), Physical Review A **98** (5), 053603.

Beattie, S., S. Moulder, R. J. Fletcher, and Z. Hadzibabic (2013), Phys. Rev. Lett. **110**, 025301.

Calderaro, L., A. L. Fetter, P. Massignan, and P. Wittek (2017), Physical Review A **95** (2), 023605.

Eckel, S., J. G. Lee, F. Jendrzejewski, N. Murray, C. W. Clark, C. J. Lobb, W. D. Phillips, M. Edwards, and G. K. Campbell (2014), Nature **506** (7487), 200.

Galitski, V., G. Juzeliūnas, and I. B. Spielman (2019), Physics Today **72** (1), 38.

Gallemí, A., A. M. Mateo, R. Mayol, and M. Guilleumas (2015), New Journal of Physics **18** (1), 015003.

Georgescu, I. (2020), Nature Reviews Physics **2** (8), 396.

Kaurov, V. M., and A. B. Kuklov (2005), Physical Review A **71** (1), 011601.

Kaurov, V. M., and A. B. Kuklov (2006), Physical Review A **73** (1), 013627.

Lamporesi, G. (2023), "Two-component spin mixtures," arXiv:2304.03711 [cond-mat.quant-gas].

Li, Y., G. I. Martone, and S. Stringari (2015), in *Annual Review of Cold Atoms and Molecules*, Annual Review of Cold Atoms and Molecules, Vol. 3 (WORLD SCIENTIFIC) pp. 201–250.

Lin, Y.-J., R. L. Compton, K. Jiménez-García, J. V. Porto, and I. B. Spielman (2009), Nature **462** (7273), 628.

Lin, Y.-J., K. Jiménez-García, and I. B. Spielman (2011), Nature **471** (7336), 83.

Pathria, R. K. (2016), *Statistical mechanics* (Elsevier).

Pitaevskii, L., and S. Stringari (2016), *Bose-Einstein condensation and superfluidity*, Vol. 164 (Oxford University Press).

Recati, A., and S. Stringari (2022), Annual Review of Condensed Matter Physics **13**, 407.

Ryu, C., M. Andersen, P. Clade, V. Natarajan, K. Helmerson, and W. D. Phillips (2007), Physical Review Letters **99** (26), 260401.

Smerzi, A., S. Fantoni, S. Giovanazzi, and S. R. Shenoy (1997), Phys. Rev. Lett. **79**, 4950.

Son, D. T., and M. A. Stephanov (2002), Phys. Rev. A **65**, 063621.

Appendix A: Numerical solutions

Our computational investigations were conducted using the Julia programming language, using public libraries suitable for technical computing tasks. Among the libraries employed, `DifferentialEquations.jl` was used to supply different time integrators for solving sets of ordinary differential equations (ODEs), and `LinearAlgebra.jl` was used in handling essential linear algebraic computations.

In particular, for the time domain, we employed the `Vern6` solver, an explicit Runge-Kutta method known for its high 6th order of accuracy and effectiveness in handling both stiff and non-stiff ODEs. Runge-Kutta methods work by taking several intermediate calculations within each time step to estimate the solution more accurately. One notable feature of the `Vern6` solver is its adaptive step size control, which allows it to dynamically adjust the step size based on the estimated error, optimizing computational resources while maintaining high precision. The time evolution typically spanned a duration of 10 times the time unit defined by the linear coupling, ensuring that the dynamics over relevant timescales were adequately captured.

In discretizing the spatial domain, we opted for a regular grid comprising 1280 points to capture the intricate dynamics of the system with high resolution. Additionally, we utilized the Fast Fourier Transform (FFT) algorithm to efficiently compute spatial derivatives, enabling us to handle periodic boundary conditions and efficiently calculate derivatives in momentum space.

Appendix B: Josephson Vortices

Josephson vortices are topological excitations in systems with linear coupling, such as two parallel coupled BECs or long Josephson junctions in superconductors (Kaurov and Kuklov, 2005). These vortices are characterized by a localized relative phase difference that leads to a supercurrent circulation around the vortex core situated in the junction (in the space between condensates).

The dynamics of JVs in a system of two coupled BECs can be described by a stationary solution to the set of linearly coupled GPEs (Baals *et al.*, 2018):

$$\begin{aligned}\psi_{\uparrow}^{(\otimes)}(x) &= \sqrt{n}\left[\tanh\left(\frac{x}{\xi_\nu}\right) + i\sqrt{1-\frac{4\nu}{gn}}\,\mathrm{sech}\left(\frac{x}{\xi_\nu}\right)\right],\\ \psi_{\downarrow}^{(\otimes)}(x) &= \left[\psi_{\uparrow}^{(\otimes)}(x)\right]^*,\end{aligned} \tag{B1}$$

where $\xi_\nu = \hbar/\sqrt{4m\nu}$ is the ν-dependent length scale of the Josephson vortex. The symbol $\otimes$ denotes the clockwise orientation of currents of the Josephson vortex (positive in component $\psi_{\uparrow}^{(\otimes)}$ and negative in $\psi_{\downarrow}^{(\otimes)}$), symbolically represented as $\uparrow\otimes\downarrow$. The typical phase profile of

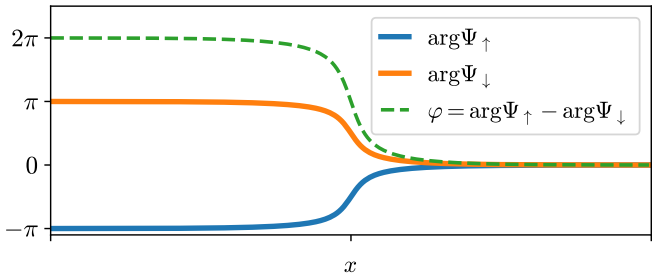

FIG. 15: Phase profile of a Josephson-vortex state.

these states is represented in Fig. 15. The energy of the JV evaluates to:

$$E_s^{\mathrm{JV}}(\nu) = \sqrt{\frac{4\nu}{gn}}\left(3 - \frac{4\nu}{gn}\right) E_{\mathrm{DS}}. \tag{B2}$$

Here E_{DS} is the energy of a dark soliton

$$\Psi_\sigma(x) = \sqrt{n}\tanh\left(\frac{x}{\xi}\right), \tag{B3}$$

characterized by the healing length $\xi = \sqrt{2\hbar^2/(mgn)}$. The study by Kaurov and Kuklov (Kaurov and Kuklov, 2005) highlights that Josephson vortices can transform into dark solitons and vice versa depending on the Josephson coupling strength ν, for $\nu < \nu_c$, the system favors Josephson vortices, whereas for $\nu > \nu_c$, dark solitons become stable. As the parameter decreases below the critical value, a DS spontaneously transforms into a JV, thereby breaking time-reversal symmetry. Conversely, as ν exceeds ν_c, the Josephson vortex transforms back into a dark soliton, restoring symmetry.